SBF
SOCIEDADE BRASILEIRA DE FÍSICA

**GENERAL AND APPLIED PHYSICS**

# Fractional Dynamics and Recurrence Analysis in Cancer Model

Enrique C. Gabrick[1] · Matheus R. Sales[1] · Elaheh Sayari[1] · José Trobia[2] · Ervin K. Lenzi[1,3] · Fernando S. Borges[4] ·
José D. Szezech Jr.[1,2] · Kelly C. Iarosz[1,5,6] · Ricardo L. Viana[6,7] · Iberê L. Caldas[7] · Antonio M. Batista[1,2,7]

**Abstract**

In this work, we analyze the effects of fractional derivatives in the chaotic dynamics of a cancer model. We begin by studying the dynamics of a standard model, i.e., with integer derivatives. We study the dynamical behavior by means of the bifurcation diagram, Lyapunov exponents, and recurrence quantification analysis (RQA), such as the recurrence rate (RR), the determinism (DET), and the recurrence time entropy (RTE). We find a high correlation coefficient between the Lyapunov exponents and RTE. Our simulations suggest that the tumor growth parameter ($\rho_1$) is associated with a chaotic regime. Our results suggest a high correlation between the largest Lyapunov exponents and RTE. After understanding the dynamics of the model in the standard formulation, we extend our results by considering fractional operators. We fix the parameters in the chaotic regime and investigate the effects of the fractional order. We demonstrate how fractional dynamics can be properly characterized using RQA measures, which offer the advantage of not requiring knowledge of the fractional Jacobian matrix. We find that the chaotic motion is suppressed as $\alpha$ decreases, and the system becomes periodic for $\alpha \lesssim 0.9966$. We observe limit cycles for $\alpha \in (0.9966, 0.899)$ and fixed points for $\alpha < 0.899$. The fixed point is determined analytically for the considered parameters. Finally, we discover that these dynamics are separated by an exponential relationship between $\alpha$ and $\rho_1$. Also, the transition depends on a supper transient which obeys the same relationship.

**Keywords** Cancer model · Fractional calculus · Recurrence analysis

All authors contributed equally to this work.

✉ Enrique C. Gabrick
ecgabrick@gmail.com

1    Graduate Program in Science, State University of Ponta Grossa, Ponta Grossa 84030-900, PR, Brazil

2    Department of Mathematics and Statistics, State University of Ponta Grossa, Ponta Grossa 84030-900, PR, Brazil

3    Department of Physics, State University of Ponta Grossa, Ponta Grossa 84030-900, PR, Brazil

4    Department of Physiology and Pharmacology, State University of New York Downstate Health Sciences University, Brooklyn 11203, NY, USA

5    University Center UNIFATEB, Telêmaco Borba 84266-010, PR, Brazil

6    Institute of Physics, University of São Paulo, São Paulo 05508-090, SP, Brazil

7    Department of Physics, Federal University of Paraná, Curitiba 82590-300, PR, Brazil

## 1 Introduction

Cancer is a set of diseases that arises from the abnormal growth and uncontrolled division of body cells. It can spread to the body's cells, causing many deaths [1]. Each year the American Cancer Society estimates the number of new cancer cases. For 2020 there was an estimated number of 19.3 million new cancer cases and almost 10.0 million deaths from cancer [2]. Only in the United States of America were projected 1,918,030 new cancer cases and 609,360 cancer deaths for 2022 [3]. In this way, cancer is a crucial public health problem worldwide [4] that requires many efforts to understand the mechanism behind the illness and improve the treatment methods [5–7]. There are several methods to study the dynamics of cancer cell proliferation and one of the most successful method is through mathematical models.

Mathematical model is a powerful tool for understanding cancer dynamics [8, 9] and simulate treatment measures, such as effects of drug resistance [10, 11], immunotherapy [12], chemotherapy [13, 14], radiotherapy [15], biochemotherapy [16] and predict fluctuations associated with the

growth rate of cancer cells [17]. A fundamental question that arises is how to understand the dynamics among healthy cells, the immune system and the tumor cells. In light of this question, several models have been proposed and studied [18–24].

Dehingia et al. [25] studied the effect of time delay in tumor-immune interaction and stimulation process. They obtained conditions for the existence of equilibrium points and Hopf bifurcation. Also, they derived conditions for periodic solutions. Díaz-Marín et al. [26] proposed a model to describe cell population dynamics in a tumor with periodic radiation as treatment. As global attractors, they found almost periodic solutions or the vanishing equilibrium. López et al. [27] formulated a model for tumor growth in the presence of cytotoxic chemotherapeutic agents. Their model allows an investigation of the Norton-Simon hypothesis in the context of dose-dense chemotherapy. In another work, López et al. [28] validated a model by means of experimental results. In this model, they considered tumor growth, including tumor-healthy cell interactions, immune response, and chemotherapy. Most of these models deal with three or more dimensional systems, where chaotic behavior is a possibility [29].

A three-dimensional cancer model with chaotic dynamics was proposed by Itik and Banks [30]. In their model, they considered the interactions of tumor cells with healthy host cells and immune systems. Through the calculation of Lyapunov exponents, they showed the existence of chaotic attractors for some parameters. Letellier et al. [31], made a topological and observability analysis of this model. They also investigated the equilibrium points and the bifurcation diagrams. Khajanchi et al. [32] studied a similar model with time delay. They analyzed the existence and stability of biologically feasible points and the emergence of Hopf bifurcations. Chaos in the 3-cell cancer model was also studied by Abernethy and Gooding [33], Gallas et al. [34], Khajanchi [35] and others [36–39].

Although the literature about the model proposed by Itik and Banks [30] is extensive, the works are restricted to integer-order differential equations. However, this formulation does not incorporate non-local effects. To do that, it is necessary to consider fractional differential equations [40]. In general, non-local operators are more efficient in describing some situations since they capture non-localities and have memory effects [41]. Fractional operators have been used to model many real problems, such as photo acoustic [42, 43], viscoelastic properties [44], Quantum Mechanics [45–47], Epidemiology [48, 49], Ecology [50, 51], Duffing oscillator [52] and many others [53–55].

The dynamical behavior of the cancer model proposed by Itik and Banks [30] was studied in light of fractional operators in Ref. [56]. It was considered three different fractional derivatives formulations: the power-law [57] (singular kernel), the exponential [58], and the Mittag-Leffler [59]. The results show that the dynamics is changed as a consequence of the extension to fractional differential operators. Ghanbari [60] also explored the same model and investigated the influence of power-law, exponential decay-law, and Mittag-Leffler in the fractal-fractional approach. These researchers obtained conditions for the existence and uniqueness of the solutions and expanded a numerical method to study the dynamical behavior. The results showed that the dynamics change from chaotic to a limit cycle depending on the factional order. Naik et al. [61], considering an extension given by the Caputo derivative, analyzed the stability of the model. In a numerical scheme, they reported that the system goes to a limit cycle in a chaotic regime for the standard model. Xuan et al. [62], using the Caputo fractal-fractional derivative in the cancer model, demonstrated that hidden attractors emerge under fractional operators. To study the system's complexity, they studied bifurcation diagrams and stability. Their findings also showed that the system converges to a limit cycle attractor when the fractional order is decreased. These works extend the model of Itik and Banks [30]. Extensions of other cancer models can be found in Refs. [63–72].

In this work, we analyze the influence of fractional operators in a cancer model [30]. As a definition of the fractional operator, we follow the Caputo scheme [41], with an order equal to $\alpha$. We consider the parameters in which the trajectories are chaotic [31]. As a novelty, we characterize the model using recurrence quantification, such as recurrence rate (RR), recurrence time entropy (RTE), and determinism (DET). Furthermore, we localize the $\alpha$ value in which the system transits from chaos to limit cycle utilizing RTE. Also, considering the mean square deviation of the time series, we construct the plane parameters composed of $\rho_1 \times \alpha$, where $\rho_1$ is the tumor growth. Our results suggest an exponential relation between $\alpha$ and tumor growth rate $\rho_1$ in which the dynamics transit from the limit cycle to a fixed point. This transition depends on a supper transient time that follows the same relationship between $\rho_1$ and $\alpha$.

Our work is organized as follows. In Sect. 2, we revisit the integer-order model analyzing the fixed points and their stabilities. Section 3 discusses the fractional influences in the cancer model. Our conclusions are drawn in Sect. 4.

## 2 Standard Model

We consider a cancer model that describes the interactions among host cells ($H$), effector immune cells ($E$) and tumor cells ($T$), governed by the following equations:

$$\frac{dH}{dt} = \rho_1 H \left(1 - \frac{H}{\kappa_1}\right) - \alpha_{13} TH, \tag{1}$$

$$\frac{dE}{dt} = \rho_2 \frac{TE}{T + \kappa_2} - \alpha_{23} TE - \delta_2 E, \tag{2}$$

$$\frac{dT}{dt} = \rho_3 T \left(1 - \frac{T}{\kappa_3}\right) - \alpha_{31} TH - \alpha_{32} TE. \tag{3}$$

Equation (1) describes the growth of the host cells by a logistic function with a rate equal to $\rho_1$ and biotic capacity equal to $\kappa_1$. The host cells are killed by tumor cells. This term is represented by the interaction $-\alpha_{13} TH$, where $\alpha_{13}$ is the host cell killing rate by tumor cells. Equation (2) gives the rate at which immune cells appear. These cells are the tumor antigens whose growth depends on the quantity of $T$, the growth rate of effector immune cells ($\rho_2$), and a positive constant $\kappa_2$. The tumor cell not only contributes to the growth of immune cells but also to its death. In the term $-\alpha_{23} TE$, $\alpha_{23}$ is the rate at which tumor cells inhibit the immune cells. In addition, the $E$ cells die according to $\delta_2$. The last equation, Eq. (3), gives the dynamics of the tumor cells. Similarly, with the $H$ cells, the tumor growth is given by a logistic function with a growth rate equal to $\rho_3$ and biotic capacity equal to $\kappa_3$. The $T$ cells are killed by $H$ cells at a rate equal to $\alpha_{31}$ and by the $E$ cells with a rate equal to $\alpha_{32}$.

Considering the transformation $(H, E, T) \rightarrow (x, y, z)$ [30], the normalized equations are

$$\frac{dx}{dt} = \rho_1 x(1 - x) - \alpha_{13} xz, \tag{4}$$

$$\frac{dy}{dt} = \frac{\rho_2 yz}{1 + z} - \alpha_{23} yz - \delta_2 y, \tag{5}$$

$$\frac{dz}{dt} = z(1 - z) - xz - \alpha_{32} yz. \tag{6}$$

A schematic representation of the model is displayed in Fig. 1. The red, green, and blue circles represent the $x$, $y$, and $z$ cells, respectively. The arrows indicate the interactions. If the interaction is constructive (growth cells), we denote with a signal +. If the interaction is destructive (kill cells), we denote it by a signal −. The $x$ cells growth with a rate $\rho_1$, which is indicated by $+\rho_1$ in Fig. 1. The $x$ cells are killed by the tumor cells at a rate equal to $\alpha_{13}$. The tumor cells grow according to a rate $\rho_3$ and are killed by $x$ cells at a rate $\alpha_{31}$ and by $y$ at a rate equal to $\alpha_{32}$. The $y$ cells grow when interacting with tumor cells by a rate $\rho_2$ and are killed by $z$
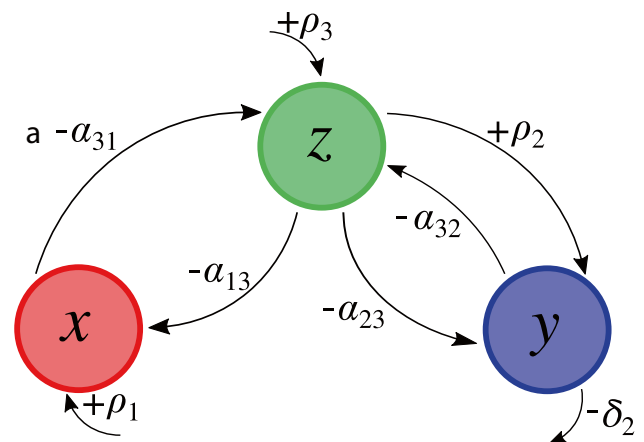


**Fig. 1** Schematic representation of the cancer model. $x$, $y$ and $z$ represent the host, immune, and tumor cells. $\rho_1$ is the growth rate of $x$, $\alpha_{13}$ is the death rate of $x$ due to $z$, $\alpha_{31}$ is the death rate of $z$ due to $x$, $\rho_3$ is the growth rate of $z$, $\alpha_{32}$ is the death rate of $z$ due to $y$, $\rho_2$ is the growth rate of $y$ due to $z$, $\alpha_{32}$ is the death rate of $y$ due to $z$ and $\delta_2$ is the natural death of $y$

cells according to a rate equal to $\alpha_{23}$. Also, the $y$ cells have a natural death $\delta_2$. The immune cells do not interact with the host cells. In this way, the tumor cells are the generalist competitors and the other two are specialist competitors [31]. In this type of interaction, there is no particular prey.

The fixed point solutions of this model are found by solving:

$$0 = \rho_1 x(1 - x) - \alpha_{13} xz, \tag{7}$$

$$0 = \frac{\rho_2 yz}{1 + z} - \alpha_{23} yz - \delta_2 y, \tag{8}$$

$$0 = z(1 - z) - xz - \alpha_{32} yz, \tag{9}$$

admitting seven solutions, that are $F_i \equiv (x^i, y^i, z^i)$, where $i = 1, ..., 7$. Solving Eqs. (7), (8), and (9), we obtain

$$F_1 = (0, 0, 0), \quad F_2 = (0, 0, 1), \quad F_3 = (1, 0, 0) \tag{10}$$

$$F_4 = \left(0, \frac{\sqrt{(\alpha_{23} + \delta_2 - \rho_2)^2 - 4\alpha_{23}\delta_2} + 3\alpha_{23} + \delta_2 - \rho_2}{2\alpha_{23}\alpha_{32}}, \right.$$
$$\left. -\frac{\sqrt{(\alpha_{23} + \delta_2 - \rho_2)^2 - 4\alpha_{23}\delta_2} + \alpha_{23} + \delta_2 - \rho_2}{2\alpha_{23}}\right) \tag{11}$$

$$F_5 = \left( \frac{\alpha_{13}\left( \sqrt{-2\rho_2(\alpha_{23}+\delta_2) + (\alpha_{23}-\delta_2)^2 + \rho_2^2} + \alpha_{23} + \delta_2 - \rho_2 \right)}{2\alpha_{23}\rho_1} + 1, \right.$$
$$-\frac{(\alpha_{13}-\rho_1)\left( \sqrt{(\alpha_{23}+\delta_2-\rho_2)^2 - 4\alpha_{23}\delta_2} + \alpha_{23} + \delta_2 - \rho_2 \right)}{2\alpha_{23}\alpha_{32}\rho_1},$$
$$\left. -\frac{\sqrt{(\alpha_{23}+\delta_2-\rho_2)^2 - 4\alpha_{23}\delta_2} + \alpha_{23} + \delta_2 - \rho_2}{2\alpha_{23}} \right),$$

$$(12)$$

$$F_6 = \left( 0, -\frac{\sqrt{(\alpha_{23}+\delta_2-\rho_2)^2 - 4\alpha_{23}\delta_2} - 3\alpha_{23} - \delta_2 + \rho_2}{2\alpha_{23}\alpha_{32}}, \right.$$
$$\left. \frac{\sqrt{(\alpha_{23}+\delta_2-\rho_2)^2 - 4\alpha_{23}\delta_2} - \alpha_{23} - \delta_2 + \rho_2}{2\alpha_{23}} \right),$$

$$(13)$$

$$F_7 = \left( \frac{\alpha_{13}\left( -\sqrt{-2\rho_2(\alpha_{23}+\delta_2) + (\alpha_{23}-\delta_2)^2 + \rho_2^2} + \alpha_{23} + \delta_2 - \rho_2 \right)}{2\alpha_{23}\rho_1} + 1, \right.$$
$$\frac{(\alpha_{13}-\rho_1)\left( \sqrt{(\alpha_{23}+\delta_2-\rho_2)^2 - 4\alpha_{23}\delta_2} - \alpha_{23} - \delta_2 + \rho_2 \right)}{2\alpha_{23}\alpha_{32}\rho_1},$$
$$\left. \frac{\sqrt{(\alpha_{23}+\delta_2-\rho_2)^2 - 4\alpha_{23}\delta_2} - \alpha_{23} - \delta_2 + \rho_2}{2\alpha_{23}} \right).$$

$$(14)$$

To simplify the analysis of the fixed points, the parameters are equal to $\alpha_{13} = 1.5, \rho_2 = 4.5, \alpha_{23} = 0.2, \delta_2 = 0.5$ and $\alpha_{32} = 2.5$. $\rho_1$ is maintained as our control parameter in the entire work. For these values, the fixed points are $F_1 = (0,0,0)$, $F_2 = (0,0,1)$, $F_3 = (1,0,0)$, $F_4 = (0, 0.3469, 0.1325)$, $F_5 = \frac{1}{\rho_1}(\rho_1 - 0.1987,$ $0.0530(1.5 - \rho_1), 0.1325\rho_1), F_6 = (0, -7.1470, 18.8675)$ and $F_7 = \frac{1}{\rho_1}(\rho_1 - 28.3012, 7.5470(1.5 - \rho_1), 18.8675\rho_1)$. $F_1$ is a trivial solution and exhibits a population without cells. The eigenvalues associated with the Jacobian calculated in $F_1$ are $(1, -0.5, \rho_1)$. The signs depend on $\rho_1$, which is always positive. Then, we find two unstable and one stable point, which characterize a saddle. $F_2$ is the point that represents a situation where the cancer cells occupy the whole host. The Jacobian eigenvalues in $F_2$ are $(1.55, \rho_1 - 1.5, -1)$. Considering $\rho_1 = 0.6$, we obtain $(1.55, -0.9, -1)$, which characterizes a saddle point. $F_3$ corresponds to the cancer-free solution. The Jacobian eigenvalues calculated at this point are $(0, -0.5, -\rho_1)$, as $\rho_1 \geq 0$, we have two negative eigenvalues and one equal zero. Thus, this point is a saddle. In $F_4$, all coordinates are positives; all solutions are in the positive octant. The Jacobian eigenvalues in this point are $(\rho_1 - 0.198754, -0.0662515 + 0.6131239\,i, -0.0662515 - 0.6131239\,i)$. The $F_5$ point has a biological significance for $\rho_1 \in [0.1987, 1.5]$. Selecting $\rho_1 = 0.6$, we obtain $(0.6688, 0.0795, 0.1325)$ which is an unstable point. The $F_6$ point has a negative term associated with the effector immune cells. Therefore, this solution does not have biological relevance. $F_7$

has a biological relevance when $\rho_1 \geq 28.3012$. However, considering this range, the second element of $F_7$ is negative. This way, the point $F_7$ is irrelevant.

The numerical solutions for Eqs. (4) (blue line), (5) (red line) and (6) (green line) are displayed in Fig. 2(a) for $\rho_1 = 0.4$, $\alpha_{13} = 1.5$, $\rho_2 = 4.5$, $\alpha_{23} = 0.2$, $\alpha_{32} = 2.5$ and $\delta_2 = 0.5$. For these parameters, the solution is a limit cycle. The solutions show that the number of host cells decreases while the immune and cancer increase. After that, the solution reaches an oscillatory behavior between the three population cells. For different $\rho_1$ values, it is possible to observe chaotic solutions. As shown in previous works [31], the dynamical system has a chaotic attractor for $\rho_1 = 0.6$, as exhibited in Fig. 2(b). Figure 2(c) shows the 2-dimensional projection together with the fixed points.

In order to distinguish periodic dynamics from chaotic ones, we use the recurrence plots (RPs), namely, recurrence quantification analysis (RQA), which remain valid under fractional operators. The RPs, introduced by Eckmann et al. [73], provide a visual representation of recurrences of the states of a system in a $d$-dimensional phase space within a small deviation $\epsilon$, as well as a quantitative analysis of the dynamical behavior exhibited by the system. For this purpose, given a trajectory $\vec{x}(t) \in \mathbb{R}^d$, we define a recurrence matrix $\mathbf{R}$ as

$$R_{ij} = H(\epsilon - \|\vec{x}(t_i) - \vec{x}(t_j)\|), \tag{15}$$

where $i,j = 1, 2, \ldots, N$, $N$ is the length of the time series, $H$ is the Heaviside unit step function, $\epsilon$ is a small threshold and $\|\vec{x}(t_i) - \vec{x}(t_j)\|$ is the spatial distance between two states, $\vec{x}(t_i)$ and $\vec{x}(t_j)$, in phase space in terms of a suitable norm.

The recurrence matrix is symmetric and binary with the elements 0 representing the non-recurrent states and the elements 1 representing the recurrent ones. Two states are recurrent when the state at $t = t_i$ is close (up to a distance
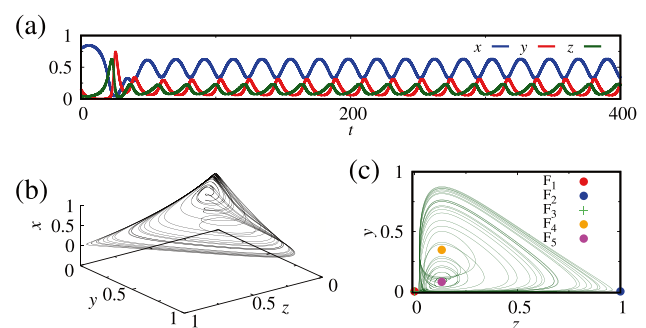


**Fig. 2** **a** Time series for $x$, $y$ and $z$ in blue, red and green lines, respectively. In panel **a**, we consider $\rho_1 = 0.4$. **b** Phase space in 3-dimensional space and projection in the plane $y - z$ in the panel **c** for $\rho_1 = 0.6$. We consider $\alpha_{13} = 1.5$, $\rho_2 = 4.5$, $\alpha_{23} = 0.2$, $\delta_2 = 0.5$, $\alpha_{32} = 2.5$, $x_0 = 0.80$, $y_0 = 0.15$, and $z_0 = 0.05$

$\epsilon$) to a different state at $t = t_j$. For the threshold $\epsilon$, we choose it to be $\epsilon = 0.01$. For a discussion on the choice of $\epsilon$, see Appendix.

Several measures based on the RPs have been proposed [74–78]. The most simple of them is the recurrence rate, RR, defined as

$$RR = \frac{1}{N^2} \sum_{i,j=1}^{N} R_{ij}, \qquad (16)$$

which is a measure of the density of recurrent points. There are also measures based on the diagonal lines formed in an RP, such as determinism (or predictability)

$$DET = \frac{\sum_{\ell=\ell_{min}}^{N} \ell P(\ell)}{\sum_{\ell=1}^{N} \ell P(\ell)}, \qquad (17)$$

where $P(\ell)$ is the total number of diagonal lines with length $\ell$ and minimal length $\ell_{min}$. Determinism is also a density as the recurrence rate. It is the density of recurrent points that lie on a diagonal line and refers to the degree to which the dynamics of a system is predictable and repeatable over time. Systems with stochastic or chaotic behaviors cause no or very short diagonal lines, whereas deterministic behavior exhibits longer diagonal lines. Therefore, the determinism is expected to be small in the first case and large in the second case. There are also measures based on the vertical lines of length $v$, such as the laminarity (LAM) and the trapping time (TT), for example. For a detailed discussion about these and other measures, see Refs. [74–78] and references therein.

Entropy-based measures of RPs have been employed to characterize the dynamical behavior of nonlinear systems [79–84, 89]. The entropy of the distribution of recurrence times (recurrence time entropy) has been utilized as a tool for the detection of chaotic orbits. The vertical distances between the diagonal lines, i.e., the gaps between them, are an estimate of the recurrence times of the trajectory [85–88]. The Shannon entropy of the distribution of white vertical lines (the estimate of the recurrence times) is defined as [79, 84, 89]

$$RTE = -\sum_{v=v_{min}}^{v=v_{max}} p_w(v) \ln p_w(v), \qquad (18)$$

where $v_{min}$ ($v_{max}$) is the length of the shortest (longest) white vertical line. $p_w(v) = P_w(v)/N_w$ and $P_w(v)$ are the relative distribution and the total number of white vertical lines of length $v$, respectively, and $N_w$ is the total number of them. Due to the finite size of a RP, the distribution of white vertical lines might be biased by the white border lines, which are cut short by the border of the RP, thus affecting the RQA measures, such as the RTE [90]. In order to avoid these border effects, it is necessary to exclude the distribution of the lines that begin and end at the border of the RP.

To investigate the dynamic behavior of the cancer model, we consider $\rho_1$ as the control parameter and compute the bifurcation diagram by recording the local maxima, $x_{max}$ (black dots) and local minima, $x_{min}$ (red dots), of $x(t)$, as shown in Fig. 3(a). For $\rho_1 < 0.5$, the dynamics is periodic and becomes chaotic via period doubling. The bifurcation diagram exhibits some periodic windows. We consider the Lyapunov exponents ($\lambda$) as a classical method to compute chaotic solutions. Figure 3(b) shows the largest, $\lambda_1$ and second largest, $\lambda_2$, Lyapunov exponents by the blue and red lines, respectively. The chaotic regimes are marked by at least one Lyapunov exponent greater than zero. In the periodic windows, we observe $\lambda_1 \approx 0$ and $\lambda_2 < 0$. On the other hand, when the dynamics is chaotic, $\lambda_1 > 0$. We also calculate the RQA measures RR, DET, and RTE in panels (c), (d), and (e), respectively. To construct the recurrence matrix, we consider the time series of $x_{max}$, $\{x_{max}^{(i)}\}_{i=1,2,...,N}$. We verify that periodic solutions exhibit large values of RR and DET, with DET $\to 1$, indicating that all recurrent points lie on a diagonal line, whereas the RTE is close to zero in these cases. RR and DET show smaller values during the chaotic windows, while the RTE is larger. Therefore, there is a correlation between $\lambda_1$ and these RQAs measures. To quantify this correlation, we use the Pearson correlation coefficient,

$$\rho_{x,y} = \frac{cov(x, y)}{\sigma_x \sigma_y}, \qquad (19)$$
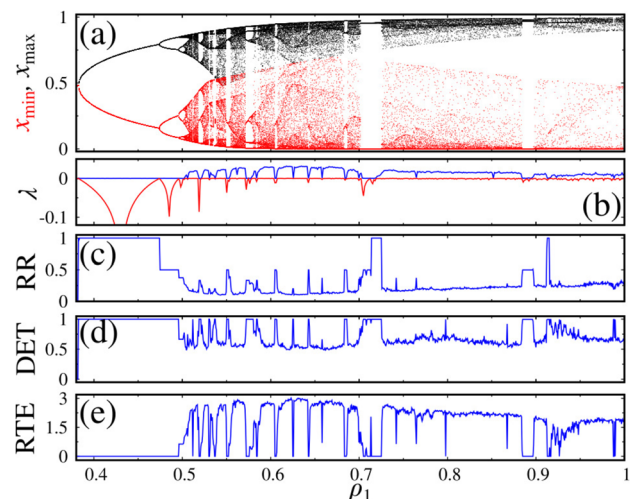


**Fig. 3 a** Bifurcation diagram of $x_{max}$ (black points) and $x_{min}$ (red points), **b** largest (blue line) and second largest Lyapunov (red line) exponents, **c** recurrence rate, RR, **d** determinism, DET, and **e** recurrence time entropy, RTE, as a function of $\rho_1$. We consider $\alpha_{13} = 1.5$, $\rho_2 = 4.5$, $\alpha_{23} = 0.2$, $\delta_2 = 0.5$, $\alpha_{32} = 2.5$, and $\epsilon = 0.01$

where $\text{cov}(x, y)$ is the covariance between the two data series and $\sigma$ their respective standard deviation. We obtain for the correlation coefficient between $\lambda_1$ and RR, DET, and RTE, the values $\rho_{\lambda_1,\text{RR}} = -0.54$, $\rho_{\lambda_1,\text{DET}} = -0.41$, $\rho_{\lambda_1,\text{RTE}} = 0.88$, respectively. Thus, the RTE is a great alternative for the characterization of the dynamics of this system.

## 3 Fractional Approach

The fractional extension of the model described by Eqs. (4), (5) and (6) is obtained by making the following substitution: $Df \rightarrow D^\alpha f$, where $D$ is the integer differential operator, i.e., $df/dt$ and $_0D_t^\alpha f$ is the fractional differential operator and is defined, in the Caputo sense, by

$$_0D_t^\alpha f \equiv \frac{1}{\Gamma(1-\alpha)} \int_0^t dt' \frac{1}{(t-t')^\alpha} \frac{\partial}{\partial t} f(\vec{r}, t), \qquad (20)$$
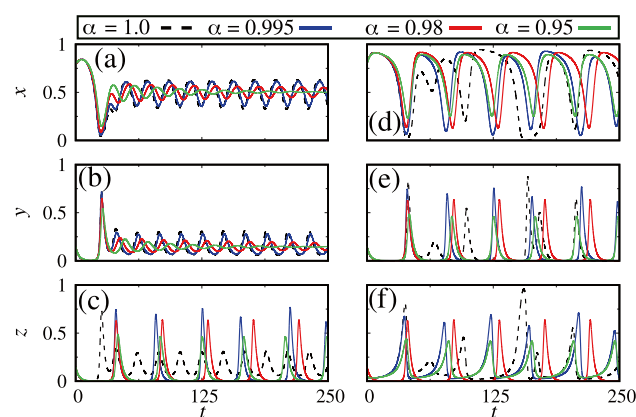
where $\Gamma(\cdot)$ is the gamma function and $0 < \alpha < 1$ [41]. Therefore, the extended cancer model is given by

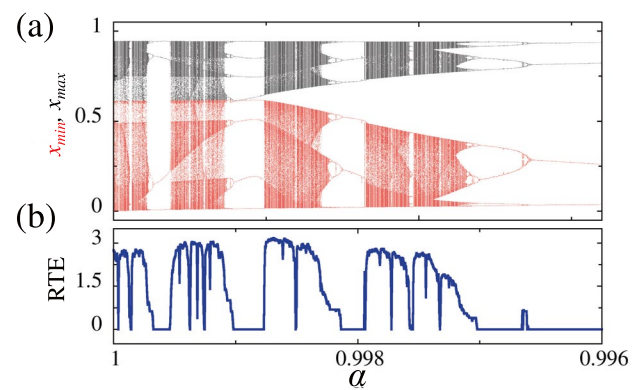$$_0D_t^\alpha x = \rho_1 x(1-x) - \alpha_{13}xz, \qquad (21)$$

$$_0D_t^\alpha y = \frac{\rho_2 yz}{1+z} - \alpha_{23}yz - \delta_2 y, \qquad (22)$$

$$_0D_t^\alpha z = z(1-z) - xz - \alpha_{32}yz. \qquad (23)$$

The time series for $\alpha = 0.995$ (blue line), $\alpha = 0.98$ (red line) and $\alpha = 0.95$ (green line) are displayed in Fig. 4. The numerical integration is made by the algorithm described in
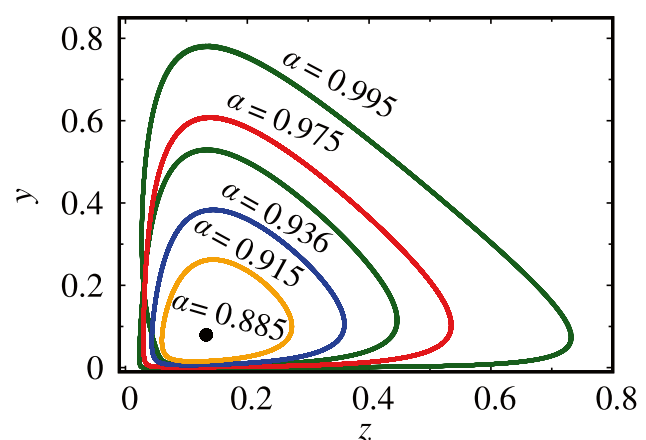


**Fig. 5** **a** RTE and **b** bifurcation diagram as a function of $\alpha$. We consider $\alpha_{13} = 1.5$, $\rho_1 = 0.6$, $\rho_2 = 4.5$, $\alpha_{23} = 0.2$, $\delta_2 = 0.5$, $\alpha_{32} = 2.5$, $x_0 = 0.80$, $y_0 = 0.15$, $z_0 = 0.05$, and $\epsilon = 0.01$

Ref. [95]. The black dotted lines are for the standard case, as exhibited in Fig. 2. These results show that the fractional order attenuates the oscillations until a fixed point as $\alpha$ decreases. For instance, for $\alpha = 0.95$, the fixed point is equal to $(x, y, z) = (0.5032, 0.1456, 0.1325)$, which corresponds to $F_5$ calculated for $\rho_1 = 0.4$.

The oscillatory behavior is attenuated in the chaotic regime for $\rho_1 = 0.6$ and the dynamics is transited to periodic behavior. By computing the RTE as a function of $\alpha$, we see that there are some periodic windows. For $\alpha \lessapprox 0.9966$, the dynamics become periodic (Fig. 5(a)). The RTE information agrees with the bifurcation diagram, as shown in Fig. 5(b). The red and black points correspond to the $x$ minimum and maximum values. The attractors in Fig. 6 display that the periodic behavior is a limit cycle that converges to a fixed



**Fig. 4** Time series for $x$ in the panels (**a**) and (**d**), for $y$ in the panels (**b**) and (**e**), and for $z$ in panels (**c**) and (**f**). The panels (**a–c**) are for $\rho_1 = 0.4$ and (**d–f**) for $\rho_1 = 0.6$. The black dotted lines are for $\alpha = 1.0$, the blue line is for $\alpha = 0.995$, the red line is for $\alpha = 0.98$ and the green line is for $\alpha = 0.95$. We consider $\alpha_{13} = 1.5$, $\rho_2 = 4.5$, $\alpha_{23} = 0.2$, $\delta_2 = 0.5$, $\alpha_{32} = 2.5$, $x_0 = 0.80$, $y_0 = 0.15$, and $z_0 = 0.05$



**Fig. 6** Phase portrait for different $\alpha$ values. The green curve is for $\alpha = 0.995$, the red curve for $\alpha = 0.975$, the blue curve for $\alpha = 0.936$, the orange curve for $\alpha = 0.915$ and the black dot for $\alpha = 0.885$. We consider $\rho_1 = 0.6$, $\alpha_{13} = 1.5$, $\rho_2 = 4.5$, $\alpha_{23} = 0.2$, $\delta_2 = 0.5$, and $\alpha_{32} = 2.5$
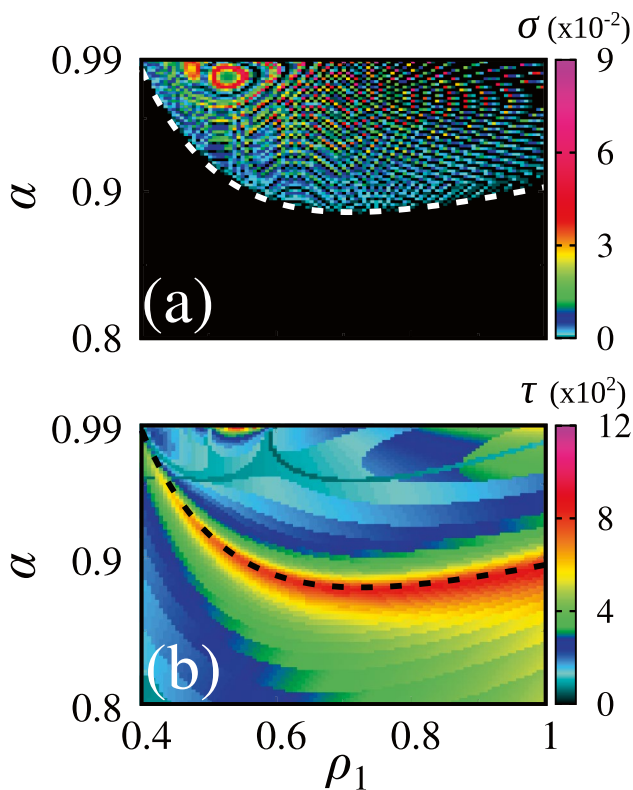
**Fig. 7** $\rho_1 \times \alpha$ as a function of $\sigma$ (mean standard deviation) in the panel (a) and $\tau$ (average transient time) in the panel (b). We consider $\alpha_{13} = 1.5$, $\rho_2 = 4.5$, $\alpha_{23} = 0.2$, $\delta_2 = 0.5$, and $\alpha_{32} = 2.5$

point as $\alpha$ approaches to 0.9. The green line is for $\alpha = 0.995$, the red line for $\alpha = 0.975$, the blue line for $\alpha = 0.936$, the orange line for $\alpha = 0.915$ and the black dotted point for $\alpha = 0.885$.
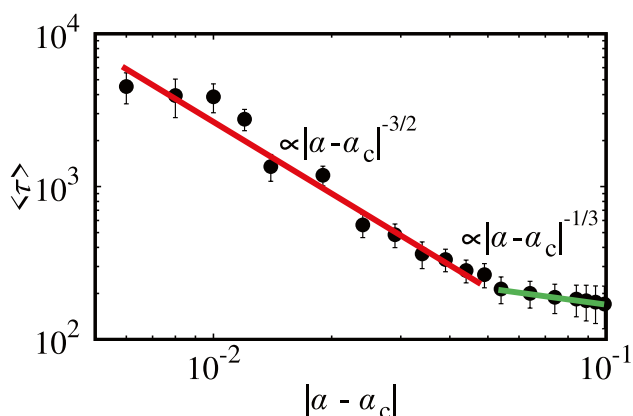


**Fig. 8** $\langle \tau \rangle$ versus $|\alpha - \alpha_c|$, where $\alpha_c = 0.899$. The curve has two slopes, in the red curve $\gamma \approx -3/2$ and in the green $\gamma \approx -1/3$. The respective correlation coefficients are 0.98 and 0.99. We consider $\rho_1 = 0.6$, $\alpha_{13} = 1.5$, $\rho_2 = 4.5$, $\alpha_{23} = 0.2$, $\delta_2 = 0.5$, and $\alpha_{32} = 2.5$

One way to differentiate fixed points and limit cycles is by computing the mean standard deviation ($\sigma$). To do that, we discard a transient time ($\tau$). Considering this time series, we compute $\sigma$. Figure 7(a) displays the parameter plane $\rho_1 \times \alpha$ as a function of $\sigma$ in color scale. The black points indicate when the solution is a fixed point ($\sigma < 10^{-3}$) and the colorful points indicate limit cycle solutions. Although some black points are mixed with colorful ones, a relation between $\alpha$ and $\rho_1$ separates most parts of the limit cycle from the fixed point solutions. This curve is indicated by the white dotted line in the panel (a) and is given by $\alpha = \beta_1 e^{\beta_2 \rho_1} + \beta_3 e^{\beta_4 \rho_1}$, where $\beta_1 = 3.150$, $\beta_2 = -7.800$, $\beta_3 = 0.808$ and $\beta_4 = 0.110$. Figure 7(b) exhibits the same plane parameter with the time to the solution for one initial condition reaches the steady solution in the color scale. The black dotted line indicates a region of super transient, which is defined by $\alpha = \xi_1 e^{\xi_2 \rho_1} + \xi_3 e^{\xi_4 \rho_1}$, where $\xi_1 = 3.25$, $\xi_2 = -7.7$, $\xi_3 = 0.802$, and $\xi_4 = 0.108$. Note that $\beta_i \approx \xi_i$. In this way, the transition from the limit cycle to fixed points crosses a supper transient region.

As our results suggest, the transition from a limit cycle to fixed points is associated with a supper transient time. In this way, we select $\rho_1 = 0.6$ and compute the mean transient time $\langle \tau \rangle$ for 100 different initial conditions close to the critical point. The critical point defines the transition and equals $\alpha_c = 0.899$. Figure 8 shows the mean transient time ($\langle \tau \rangle$) as a function of $|\alpha - \alpha_c|$ by the black points. The average transient lifetime scales with $\alpha$ as a power-law according to

$$\langle \tau \rangle \propto |\alpha - \alpha_c|^\gamma, \tag{24}$$

and has two slopes. By fitting the data (red line in Fig. 8), we obtain an exponent of $\gamma \approx -3/2$, with a correlation coefficient of 0.98 and $\gamma \approx -1/3$ (green line) with a correlation coefficient of 0.99. All the points evolve to $F_5$.

## 4 Conclusions

In this work, we consider a fractional extension of a cancer model. This model describes the interactions among host, effector immune, and tumor cells. Due to the non-linearity, the dynamical behavior exhibits chaotic solutions for some parameter ranges. For the equations that govern the model, we obtain analytical solutions for the fixed points and discuss their stability.
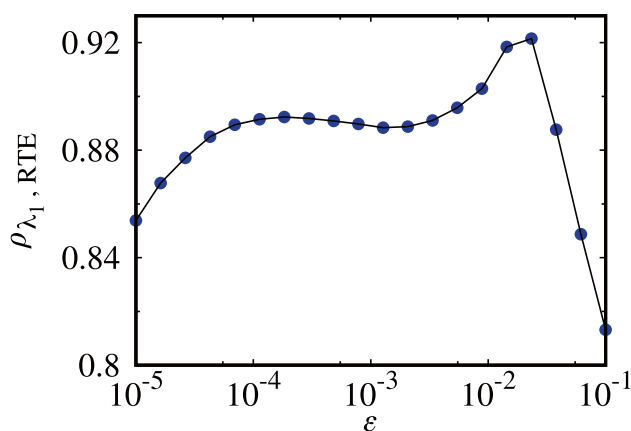
In order to study a more broad case, we consider numerical solutions. As previously reported works, we verify chaotic solutions for $\rho_1 = 0.6$. Furthermore, we construct bifurcation diagrams considering the maxima and minimum points of the host cells. The dynamical behavior exhibited by the bifurcation diagram also was verified by

the Lyapunov exponents and recurrence quantification analysis (RQA) measures. With regard to the RQA measures, we compute the recurrence rate (RR), determinism (DET), and recurrence time entropy (RTE). All three of them agree with the results from the Lyapunov exponents. By computing the Pearson correlation coefficient between them and $\lambda_1$, we observe a higher coefficient for the RTE. Thus, we consider only the RTE to analyze the effects of fractional order.

We study the effects of fractional operators in the cancer model by the Caputo definition. Our main goal is to understand what happens in the chaotic behavior. By computing the RTE, our results suggest that the dynamical system becomes periodic for $\alpha \lessgtr 0.9966$. When we look for the phase portrait, the results show that the solutions transit from a limit cycle to a fixed point, which is equal to the fixed points calculated analytically. The limit cycle regime is in the range $\alpha \in (0.9966, 0.899)$ for $\rho_1 = 0.6$. For different $\rho_1$ values, we construct the parameter space $\rho_1 \times \alpha$ as a function of the mean standard deviation $\sigma$. Values of $\sigma$ close to zero show fixed point solutions. Our results show the existence of an exponential curve that delimits fixed point solutions from limit cycles in this parameter space. Also, we analyze the transient time related to the transition from the limit cycle to a fixed point. For $\rho_1 = 0.6$, we find that for $\alpha < 0.899$ the dynamics go to the fixed point $F_5$ by a super transient with order $10^4$. The super transient curve follows a linear decay according to two slopes, equal to $-3/2$ and $-1/3$.

# Appendix

In Sect. 2, we introduced the cancer model and analyzed its dynamics for different parameter values by means of a bifurcation diagram, the Lyapunov exponents, and three RQA

measures: RR, DET, and RTE. We chose the threshold $\epsilon$ to be $\epsilon = 0.01$. Many researchers have addressed the problem of finding the best value of $\epsilon$ [91–94]. Here, we used the correlation coefficient, Eq. (19), to determine $\epsilon$. We computed the RTE as a function of $\rho_1$ for different threshold values, ranging from $10^{-5}$ to $10^{-1}$, and calculated the correlation coefficient between $\lambda_1$ and RTE (Fig. 9). Even if we choose a very small $\epsilon$ ($10^{-5}$) or a relatively large $\epsilon$ ($10^{-1}$), we still obtain a rather high correlation coefficient, with the highest value being around $\epsilon \approx 10^{-2}$, and hence our choice of $\epsilon$. Furthermore, the fact that $\rho_{\lambda_1, \text{RTE}}$ does not change too much within this range of $\epsilon$ indicates that, in our case, the choice of $\epsilon$ is not as sensible as it would be in other cases. In fact, there is a wide range of values for $\epsilon$ in which the results are good.

## Declarations

**Conflict of Interest** The author declares that there exists no competing financial interest or personal relationships that could have appeared to influence the work reported in this paper.



**Fig. 9** The correlation coefficient between $\lambda_1$ and RTE as a function of the threshold $\epsilon$

## References

1. D.M. Hausman, What is cancer? Perspect. Biol. Med. **62**(4), 778–784 (2019)
2. J. Ferlay, M. Colombet, I. Soerjomataram, D.M. Parkin, M. Piñeros, A. Znaor, F. Bray, Cancer statistics for the year 2020: An overview. Cancer Epidemiol. **149**, 778–789 (2021)
3. R.L. Siegel, K.D. Miller, H.E. Fuchs, A. Jemal, Cancer statistics, 2022. CA Cancer J. Clin. **72**, 7–33 (2022)
4. R.L. Siegel, K.D. Miller, A. Jemal, Cancer statistics, 2018. CA Cancer J. Clin. **68**, 7–30 (2018)
5. P.A. Jones, S.B. Baylin, The epigenomics of cancer. Cell **128**, 683–692 (2007)
6. C. Mufudza, W. Sorofa, E.T. Chiyaka, Assessing the effects of estrogen on the dynamics of breast cancer. Comput. Math. Methods Med. **2012**, 473572 (2012)
7. A.D. Waldman, J.M. Fritz, M.J. Lenardo, A guide to cancer immunotherapy: From T cell basic science to clinical practice. Nat. Rev. Immunol. **20**, 651–668 (2020)
8. A.G. López, J.M. Seoane, M.A.F Sanjuán, in *Advanced Mathematical Methods in Biosciences and Applications*, ed. by F.

Berezovskaya, B. Toni. Modelling cancer dynamics using cellular automata (2019), pp. 159–205

9. K.C. Iarosz, F.S. Borges, A.M. Batista, M.S. Baptista, R.A.N. Siqueira, R.L. Viana, S.R. Lopes, Mathematical model of brain tumour with glia-neuron interactions and chemotherapy treatment. J. Theor. Biol. **368**, 113–121 (2015)

10. J. Trobia, E.C. Gabrick, E.G. Seifert, F.S. Borges, P.R. Protachevicz, J.D. Szezech Jr., K.C. Iarosz, M.S. Santos, I.L. Caldas, K. Tian, H.P. Ren, C. Grebogi, A.M. Batista, Effects of drug resistance in the tumour-immune system with chemotherapy treatment. Indian Acad. Sci. Conf. Ser. **3**(1), 39–44 (2020)

11. J. Trobia, K. Tian, A.M. Batista, C. Grebogi, H.P. Pen, M.S. Santos, P.R. Protachevicz, F.S. Borges, J.D. Szezech Jr., R.L. Viana, I.L. Caldas, K.C. Iarosz, Mathematical model of brain tumour growth with drug resistance. Commun. Nonlinear Sci. Numer. Simul. **103**, 106013 (2021)

12. F. Castiglione, B. Piccoli, Cancer immunotherapy, mathematical modeling and optimal control. J. Theor. Biol0 **247**(4), 723–732 (2007)

13. A.G. López, K.C. Iarosz, A.M. Batista, J.M. Seoane, R.L. Viana, M.A.F. Sanjuán, The role of dose density in combination cancer chemotherapy. Commun. Nonlinear Sci. Numer. Simul. **79**, 104918 (2019)

14. F.S. Borges, K.C. Iarosz, H.P. Ren, A.M. Batista, M.S. Baptista, R.L. Viana, S.R. Lopes, C. Grebogi, Model for tumour growth with treatment by continuous and pulsed chemotherapy. Biosystems **116**, 43–48 (2014)

15. Z. Liu, C. Yang, A Mathematical Model of Cancer Treatment by Radiotherapy. Comput. Math. Methods Med. **2014**, 172923 (2014)

16. M. Mamat, A.K. Subiyanto, Mathematical model of cancer treatments using immunotherapy, chemotherapy and biochemotherapy. Appl. Math. Sci. **7**(5), 247–261 (2013)

17. E. Sayari, S.T. da Silva, K.C. Iarosz, R.L. Viana, J.D. Szezech Jr., A.M. Batista, Prediction of fluctuations in a chaotic cancer model using machine learning. Chaos Solit. Fractals **164**, 112616 (2022)

18. L.G. de Pillis, A. Radunskaya, The dynamics of an optimally controlled tumor model: a case study. Math. Comput. Model. **37**, 1221–1244 (2003)

19. K.C. Iarosz, C.C. Martins, A.M. Batista, R.L. Viana, S.R. Lopes, I.L. Caldas, T.J.P. Penna, On a cellular automaton with time delay for modelling cancer tumors. J. Phys: Conf. Ser. **285**, 012015 (2011)

20. V.A. Kuznetsov, I.A. Makalkin, M.A. Taylor, A.S. Perelson, Nonlinear dynamics of immunogenic tumors: Parameter estimation and global bifurcation analysis. Bullet. Math. Biol. **56**(2), 295–321 (1994)

21. S.T.R. Pinho, H.I. Freedman, F. Nani, A chemotherapy model for the treatment of cancer with metastasis. Math. Comput. Model. Int. J. **36**(7–8), 773–803 (2002)

22. J.F. Amatruda, J.L. Shepard, H.W. Stern, L.I. Zon, Zebrafish as a cancer model system. Cancer Cell **1**(3), 229–231 (2002)

23. P.M. Altrock, L.L. Liu, F. Michor, The mathematics of cancer: Integrating quantitative models. Nat. Rev. Cancer **15**, 730–745 (2015)

24. D. Tuveson, H. Clevers, Cancer modeling meets human organoid technology. Science **364**(6444), 952–955 (2019)

25. K. Dehingia, H.K. Sarmah, Y. Alharbi, K. Hosseini, Mathematical analysis of a cancer model with time-delay in tumor-immune interaction and stimulation processes. Adv. Difference Equ. **2021**, 473 (2021)

26. H. Díaz-Marín, J.F. López-Hernández, O. Osuna, Stability and eradication of tumor in a model with almost periodically radiated cells. J. Appl. Math. Comput. **68**, 3781–3797 (2022)

27. A.G. López, K.C. Iarosz, A.M. Batista, J.M. Seoane, R.L. Viana, M.A.F. Sanjuán, Nonlinear cancer chemotherapy: Modelling the Norton-Simon hypothesis. Commun. Nonlinear Sci. Numer. Simul. **70**, 307–317 (2019)

28. A.G. López, J.M. Seoane, M.A.F. Sanjuán, A validated mathematical model of tumor growth including tumor-host interaction,

29. cell-mediated immune response and chemotherapy. Bull. Math. Biol. **76**, 2884–2906 (2014)

29. T. Tél, M. Gruiz, Chaotic dynamics: an introduction based on classical mechanics (Cambridge University Press, 2006)

30. M. Itik, S.P. Banks, Chaos in a three-dimensional cancer model. Int. J. Bifurcat. Chaos **20**(1), 71–79 (2010)

31. C. Letellier, F. Denis, L.A. Aguirre, What can be learned from a chaotic cancer model? J. Theor. Biol. **322**, 7–16 (2013)

32. S. Khajanchi, M. Perc, D. Gosh, The influence of time delay in a chaotic cancer model. Chaos Interdisc. J. Nonlinear Sci. **28**, 103101 (2018)

33. S. Abernethy, R.J. Gooding, The importance of chaotic attractors in modelling tumour growth. Physica A **507**, 268–277 (2018)

34. M.R. Gallas, M.R. Gallas, J.A.C. Gallas, Distribution of chaos and periodic spikes in a three-cell population model of cancer. Eur. Phys. J. Special Topics **223**, 2131–2144 (2014)

35. S. Khajanchi, Bifurcation analysis of a delayed mathematical model for tumor growth. Chaos Solit. Fractals **77**, 264–276 (2015)

36. F.F. Kemwoue, J.M. Dongo, R.N. Mballa, C.L. Gninzanlong, M.W. Kemayou, B. Mokhtari, F. Biya-Motto, J. Atangana, Bifurcation, multistability in the dynamics of tumor growth and electronic simulations by the use of Pspice. Chaos Solit. Fractals **134**, 109689 (2020)

37. J. Li, X. Xie, Y. Chen, D. Zhang, Complex dynamics of a tumor-immune system with antigenicity. Appl. Math. Comput. **400**, 126052 (2021)

38. P.A. Valle, L.N. Coria, D. Gamboa, C. Plata, Bounding the dynamics of a chaotic-cancer mathematical model. Math. Prob. Eng. **2018**, 9787015 (2018)

39. A. Uthamacumaran, A review of dynamical systems approaches for the detection of chaotic attractors in cancer networks. Patterns **2**(4), 100226 (2021)

40. L.R. Evangelista, E.K. Lenzi, An introduction to anomalous diffusion and relaxation (Springer Nature, 2023)

41. L.R. Evangelista, E.K. Lenzi. Fractional diffusion equations and anomalous diffusion (Cambridge University Press, 2018)

42. A. Somer, S. Galovic, E.K. Lenzi, A. Novatski, K. Djordjevic, Temperature profile and thermal piston component of photoacoustic response calculated by the fractional dual-phase-lag heat conduction theory. Int. J. Heat Mass Transf. **203**, 123801 (2023)

43. A. Somer, M.N. Popovic, G.K. da Cruz, A. Novatski, E.K. Lenzi, S.P. Galovic, Anomalous thermal diffusion in two-layer system: The temperature profile and photoacoustic signal for rear light incidence. Int. J. Therm. Sci. **179**, 107661 (2022)

44. W.P. do Carmo, A.F. Santos, M.K. Lenzi, M. Fortuny, E.K. Lenzi, A new fractional model applied to description of the viscoelastic creep behavior of two Brazilian oils and their w/o emulsions. Digital Chem. Eng. **6**, 100069 (2023)

45. D. Cius, L. Menon Jr., M.A.F. dos Santos, A.S.M. de Castro, F.M. Andrade, Unitary evolution for a two-level quantum system in fractional-time scenario. Phys. Rev. E **106**, 054126 (2022)

46. E.K. Lenzi, H.V. Ribeiro, M.A.F. dos Santos, R. Rossato, R.S. Mendes, Time dependent solutions for a fractional Schrödinger equation with delta potentials. J. Math. Phys. **54**(8), 082107 (2013)

47. E.C. Gabrick, E. Sayari, A.S.M. de Castro, J. Trobia, A.M. Batista, E.K. Lenzi, Fractional Schrödinger equation and time dependent potentials. Commun. Nonlinear Sci. Numer. Simul. 107275 (2023)

48. H.M. Srivastava, K.M. Saad, M.M. Khader, An efficient spectral collocation method for the dynamic simulation of the fractional epidemiological model of the Ebola virus. Chaos Solit. Fractals **140**, 110174 (2020)

49. N.P. Dong, H.V. Long, A. Khastan, Optimal control of a fractional order model for granular SEIR epidemic with uncertainty. Commun. Nonlinear Sci. Numer. Simul. **88**, 105312 (2020)

50. A. Kumar, S. Kumar, A study on eco-epidemiological model with fractional operators. Chaos Solit Fractals **156**, 111697 (2022)

51. E.E. Mahmoud, P. Trikha, L.S. Jahanzaib, O.A. Almaghrabi, Dynamical analysis and chaos control of the fractional chaotic ecological model. Chaos Solit. Fractals **141**, 110348 (2020)

52. M. Coccolo, J.M. Seoane, S. Lenci, M.A.F. Sanjuán, Fractional damping effects on the transient dynamics of the Duffing oscillator. Commun. Nonlinear Sci. Numer. Simul. **117**, 106959 (2023)

53. M. Nadeem, H. Jafari, A. Akgül, M. De la Sen, A computational scheme for the numerical results of time-fractional Degasperis-Procesi and Camassa-Holm models. Symmetry **14**(12), 2532 (2022)

54. G. Vivekanandhan, H.R. Abdolmohammadi, H. Natiq, K. Rajagopal, S. Jafari, H. Namazi, Dynamic analysis of the discrete fractional-order Rulkov neuron map. Math. Biosci. Eng. **20**(3), 4760–4781 (2023)

55. H.G. Sun, Y. Zhang, D. Baleanu, W. Chen, Y. Chen, A new collection of real world applications of fractional calculus in science and engineering. Commun. Nonlinear Sci. Numer. Simul. **64**, 213–231 (2018)

56. A. Atangana, S. Jain, The role of power decay, exponential decay and Mittag-Leffler function's waiting time distribution: Application of cancer spread. Phys. A **512**, 330–351 (2018)

57. M. Caputo, M. Fabrizio, On the singular kernels for fractional derivatives. Some applications to partial differential equations. Prog. Fract. Differ. Appl. **7**(2), 79–82 (2021)

58. M. Caputo, M. Fabrizio, A new definition of fractional derivative without singular kernel. Prog. Fract. Differ. Appl. **1**(2), 73–85 (2015)

59. A. Atangana, D. Baleanu, New fractional derivatives with non-local and non-singular kernel: Theory and application to heat transfer model. Therm. Sci. **20**(2), 763–769 (2016)

60. B. Ghanbari, On the modeling of the interaction between tumor growth and the immune system using some new fractional and fractional-fractal operators. Adv. Difference Equ. **2020**, 585 (2020)

61. P.A. Naik, J. Zu, M. Naik, Stability analysis of a fractional-order cancer model with chaotic dynamics. Int. J. Biomath. **14**(6), 2150046 (2021)

62. L. Xuan, S. Ahmad, A. Ullah, S. Saifullah, A. Akgül, H. Qu, Bifurcations, stability analysis and complex dynamics of Caputo fractal-fractional cancer model. Chaos Solit. Fractals **159**, 112113 (2022)

63. S. Ahmad, A. Ullah, T. Abdeljawad, A. Akgül, N. Mlaiki, Analysis of fractal-fractional model of tumor-immune interaction. Results Phys. **25**, 104178 (2021)

64. E. Ahmed, A.H. Hashis, F.A. Rihan, On fractional order cancer model. J. Fractional Calc. Appl. **3**(2), 1–6 (2012)

65. M. Arfan, K. Shah, A. Ullah, M. Shutaywi, P. Kumam, Z. Shah, On fractional order model of tumor dynamics with drug interventions under nonlocal fractional derivative. Results Phys. **21**, 103783 (2021)

66. D. Baleanu, A. Jajarmi, S.S. Sajjadi, D. Mozyrska, A new fractional model and optimal control of a tumor-immune surveillance with non-singular derivative operator. Chaos **29**, 083127 (2019)

67. N. Debbouche, A. Ouannas, G. Grassi, A.B.A. Al-Hussein, F.R. Tahir, K.M. Saad, H. Jahanshahi, A.A. Aly, Chaos in cancer tumor growth model with commensurate and incommensurate fractional-order derivatives. Comput. Math. Methods Med. **2022**, 5227503 (2022)

68. H. Hassani, J.A.T. Machado, Z. Avazzadeh, E. Safari, S. Mehrabi, Optimal solution of the fractional order breast cancer competition model. Sci. Rep. **11**, 15622 (2021)

69. O.S. Iyiola, F.D. Zaman, A fractional diffusion equation model for cancer tumor. AIP Adv. **4**, 107121 (2014)

70. S. Kumar, A. Kumar, B. Samet, J.F. Gómez-Aguilar, M.S. Osman, A chaos study of tumor and effector cells in fractional tumor-immune model for cancer treatment. Chaos Solit. Fractals **141**, 110321 (2020)

71. M.A.U. Rehaman, J. Ahmad, A. Hassan, J. Awrejcewicz, W. Pawlowski, H. Karamti, F.M. Alharbi, The dynamics of a fractional-order mathematical model of cancer tumor disease. Symmetry **14**, 1694 (2022)

72. J.E. Solís-Pérez, J.F. Gómez-Aguilar, A. Atangana, A fractional mathematical model of breast cancer competition model. Chaos Solit. Fractals **127**, 38–54 (2019)

73. J.P. Eckmann, S.O. Kamphorst, D. Ruelle, Recurrence plots of dynamical systems. Europhys. Lett. **4**(9), 973 (1987)

74. N. Marwan, N. Wessel, U. Meyerfeldt, A. Schirdewan, J. Kurths, Recurrence-plot-based measures of complexity and their application to heart-rate-variability data. Phys. Rev. E **66**(2), 026702 (2002)

75. N. Marwan, J. Kurths, Nonlinear analysis of bivariate data with cross recurrence plots. Phys. Lett. A **302**(5), 299–307 (2002)

76. N. Marwan, A historical review of recurrence plots. Eur. Phys. J. Special Topics **164**(1), 3–12 (2008)

77. G. Bedartha, A brief introduction to nonlinear time series analysis and recurrence plots. Vibration **2**(4), 332–368 (2019)

78. N. Marwan, C.L. Webber, Mathematical and computational foundations of recurrence quantifications (Springer International Publishing, 2015)

79. M.A. Little, P.E. McSharry, S.J. Roberts, D.A.E. Costello, I.M. Moroz, Exploiting nonlinear recurrence and fractal scaling properties for voice disorder detection. Biomed. Eng. Online **6**(1), 23 (2007)

80. C.L. Webber, J.P. Zbilut, Dynamical assessment of physiological systems and states using recurrence plot strategies. J. Appl. Physiol. **76**(2), 965–973 (1994)

81. L.L. Trulla, A. Giuliani, J.P. Zbilut, C.L. Webber, Recurrence quantification analysis of the logistic equation with transients. Phys. Lett. A **223**(4), 255–260 (1996)

82. E.J. Ngamga, D.V. Senthilkumar, J. Kurths, Dynamics between order and chaos revisited. Eur. Phys. J. Special Topics **191**(1), 15–27 (2010)

83. D. Eroglu, T.K.D.M. Peron, N. Marwan, F.A. Rodrigues, L.F. Costa, M. Sebek, I.Z. Kiss, J. Kurths, Entropy of weighted recurrence plots. Phys. Rev. E **90**(4), 042919 (2014)

84. M.R. Sales, M. Mugnaine, D. Szezech Jr., R.L. Viana, I.L. Caldas, N. Marwan, J. Kurths, Stickiness and recurrence plots: An entropy-based approach. Chaos Interdisc. J. Nonlinear Sci. **33**(3), 033140 (2023)

85. Y. Zou, M. Thiel, M.C. Romano, J. Kurths, Characterization of stickiness by means of recurrence. Chaos Interdisc. J. Nonlinear Sci. **17**(4) (2007)

86. Y. Zou, D. Pazó, M.C. Romano, M. Thiel, J. Kurths, Distinguishing quasiperiodic dynamics from chaos in short-time series. Phys. Rev. E **76**(1), 016210 (2007)

87. M.S. Baptista, E.J. Ngama, P.R.F. Pinto, M. Brito, J. Kurths, Kolmogorov-Sinai entropy from recurrence times. Phys. Lett. A **374**(9), 1135–1140 (2010)

88. E.J. Ngamga, D.V. Senthilkumar, A. Prasad, P. Parmananda, N. Marwan, J. Kurths, Distinguishing dynamics using recurrence-time statistics. Phys. Rev. E **85**(2), 026217 (2012)

89. K.H. Kraemer, R.V. Donner, J. Heitzig, N. Marwan, Recurrence threshold selection for obtaining robust recurrence characteristics in different embedding dimensions. Chaos Interdisc. J. Nonlinear Sci. **28**(8), 085720 (2018)

90. K.H. Kraemer, N. Marwan, Border effect corrections for diagonal line based recurrence quantification analysis measures. Phys. Lett. A **383**(34), 125977 (2019)

91. J.P. Zbilut, J.M. Zaldivar-Comenges, F. Strozzi, Recurrence quantification based Liapunov exponents for monitoring divergence in experimental data. Phys. Lett. A **297**(3), 173–181 (2002)

92. M. Thiel, M.C. Romano, J. Kurths, R. Meucci, E. Allaria, F.T. Arecchi, Influence of observational noise on the recurrence quantification analysis. Physica D **171**(3), 138–152 (2002)

93. S. Schinkel, O. Dimigen, N. Marwan, Selection of recurrence threshold for signal detection. Eur. Phys. J. Special Topics **164**(1), 45–53 (2008)

94. J. Medrano, A. Kheddar, L. Annick, R. Sofiane, Radius selection using kernel density estimation for the computation of nonlinear measures. Chaos Interdisc. J. Nonlinear Sci. **31**(8), 083131 (2021)

95. R. Garrappa, Numerical solution of fractional differential equations: a survey and a software tutorial. Mathematics **6**(16), 1–23 (2018)